Available online at www.sciencedirect.com
SCIENCE DIRECT
Journal of Molecular Catalysis A: Chemical 247 (2006) 7–13
JOURNAL OF MOLECULAR CATALYSIS A: CHEMICAL
www.elsevier.com/locate/molcata

Study of ruthenium oxide catalyst for electrocatalytic performance in oxygen evolution

Hongchao Ma, Changpeng Liu, Jianhui Liao, Yi Su, Xingzhong Xue, Wei Xing *

Changchun Institute of Applied Chemistry, Chinese Academy of Sciences, Changchun 130022, PR China

Received 1 June 2005; received in revised form 1 November 2005; accepted 1 November 2005
Available online 20 December 2005

Abstract

The RuO_2 anode catalyst for water electrolysis was prepared by a pyrolysis process in a nitrate melt at 300 °C and then calcined at different temperature from 350 to 550 °C. The physio-chemical properties of RuO_2 catalysts were examined by XRD, FE-SEM, CV, EIS, BET, etc. The impedance results in oxygen evolution region clearly show that the electrocatalytic activity of RuO_2 material decreases with the increase of calcining temperature. The resistance of catalyst layer (R_f), however, decreases with increase of calcining temperature. Thus, optimum calcining conditions are found at 350 °C, where the total polarization reaches a minimum in higher current density (>200 mA cm^{-2}). Furthermore, the RuO_2 anode also displays better stability at higher current density (1.1 A cm^{-2}) in the PEM based electrolysers.

Keywords: RuO_2; Thermal treatment; Water electrolysis; Oxygen evolution

1. Introduction

Dimensionally stable anode (DSA) with RuO_2-TiO_2 as a catalytically active layer coated on a titanium substrate by the thermal decomposition method has been successfully used and caused a technological revolution in the chlor-alkali industry since its invention in 1960s [1]. The first fundamental research on the properties of RuO_2, the main component of DSA, appeared in the open literature only in 1971 [2].

Since then, fundamental investigations of RuO_2 as anodes have increased exponentially, one of the new directions in this field is to develop RuO_2 anodes for the application in oxygen evolving conditions such as electroplating, electrowinning, electrofloatation, electrosynthesis, cathodic protection, water electrolysis, etc. [3–9].

In a future energy scenario based on renewable energy, hydrogen is an attractive energy carrier, which can be used as a non-toxic energy storage and transport medium. Hydrogen production by water electrolysis is a clean and simple way of storing energy from sources such as solar, wind and hydroelectric power. The hydrogen can then subsequently be utilized in a range of fuel cells without concern of contaminants such as carbon monoxide, which is present in reformed hydrogen.

Water electrolysis is traditionally carried out in alkaline media with many commercial electrolysers available on the market. Advanced water electrolysers using proton exchange membranes (PEM) are less common and generally utilize expensive materials such as noble metal electrocatalysts and sulphonated polymers of perfluorocarbon chains as the proton exchange membranes. The benefits of PEM based electrolysers over alkaline systems is the much higher current densities (1–3 A cm^{-2} compared with 0.2 A cm^{-2} [10,11]), no circulating liquid electrolyte, wide range of power loadings and very rapid power-up/power-down rates. The first electrolyser using polymer membrane as electrolyte was developed by General Electric Co. in 1966 for space applications [12]. Extensive research and development on SPE electrolysers has been performed by Japanese WE-NET program and other investigators [13–17].

The oxygen electrode has attracted great interest because it is the main source of overpotential in this system. Because non-noble metals like Ni and Co will corrode and Pt will be oxidated to low-conducting oxide when as anode catalysts in acidic Nafion membrane have been used as electrolyte. Thus, the oxides of noble metals Ru and Ir due to their high ohmic conductivity, chemical and thermal stability have been more used as anodic catalysts.

* Corresponding author. Tel.: +86 431 5262223; fax: +86 431 5262225.
E-mail address: xingwei@ciac.jl.cn (W. Xing).

1381-1169/$ – see front matter © 2005 Elsevier B.V. All rights reserved.
doi:10.1016/j.molcata.2005.11.013

In the present work, the RuO_2 catalysts were prepared from $RuCl_3 \cdot nH_2O$ using the Adams fusion method [18] and then calcined at various temperatures. We are focusing on the effect of thermal treatment on structures and performance of oxygen evolution of RuO_2 anode such as electrochemical active area, film resistance (R_f), charge transferred resistance (R_{ct}), etc.

2. Experimental

A fresh hydrated $RuCl_3$ (Ru assay = 37.2%) by SPM Co. Ltd. was used. Nafion membrane and Nafion solution from Du Pont and 40 wt% Pt/C made in self. Nitrate sodium of analytical purity was supplied by Beijing chemical industry plant. All the water used was tapped from a Milli-Q Ultra Pure Water system with a water resistivity of 18.2 MΩ cm.

2.1. Preparation of RuO_2 catalyst

RuO_2 catalysts were prepared from $RuCl_3 \cdot nH_2O$ using the Adams fusion method [18]. In our preparation 1 g of metal chloride precursor was mixed in an excess of 20 g of $NaNO_3$ and dissolved in water. The water was gradually evaporated from the mixture and the salt mixture was introduced into a ceramic furnace, pre-heated at 300 °C for 3 h, then the salt mixture was cooled to room temperature and washed in water to remove impurities. The resulting metal oxide was then dried and calcined at a predetermined time and temperature.

2.2. Preparation of MEAs

The anodic and cathodic electrodes were prepared by a brushing procedure using catalysts, carbon powder (Vulcan XC-72, Cabot), a carbon paper substrate, a polytetrafluoroethylene (PTFE) suspension (Teflon 306A, Du Pont) and a 5 wt% Nafion solution (Aldrich).

A homogeneous suspension composed of PTFE and carbon powder was brushed onto the carbon paper (geometric area of 9 cm^2) to form the diffusion layer (thickness about 100 μm) of the electrodes [19,20]. The composite structure was then dried in air at 120 °C for 30 min followed by thermal treatment in air at 350 °C for 30 min to remove the dispersion agent contained in PTFE. The amount of PTFE in the diffusion layer was 20 wt%.

To prepare the catalyst layer, a homogeneous suspension was formed from the RuO_2 or 40 wt% Pt/C catalyst and the Nafion solution with isopropanol as solvent. The resulting ink was deposited onto the composite diffusion layer of the electrode by a brushing procedure to produce the catalyst layer. RuO_2 loading, platinum loading and Nafion content were 10, 0.4 and 1 mg cm^{-2} in slurry, respectively. After pretreatment of the Nafion membrane with H_2O_2/H_2SO_4, electrodes and membrane have been hot-pressed (4 MPa, 120 °C) for 3 min.

The single SPE cell body was made of gilded Ti with flow fields machined into the Ti plates. Gilded Ti-net functioned as backings and was pressed by the Ti plates against the MEAs.

2.3. Electrochemical measurements and characterization of RuO_2

Applying a three-electrode cell with one reference electrode is extremely difficult for the investigation of electrochemical systems with solid electrolytes, furthermore Marshall et al. [21] also reported that oxide catalysts have similarly behaves in aqueous and PEM cell.

Thus, cyclic voltammetry (CV) studies were performed with a PAR 273A potentiostat/galvanostat in a three-electrode configuration using a platinum plate counterelectrode and a saturated silver-chloride reference electrode. The working electrode was prepared by mixing the active material with 5 wt% Nafion ionomer in ethanol solvent, which was made into slurry. A small drop of the slurry was added on to the mirror polished glassy-carbon substrate. The electrolyte was 1 M H_2SO_4 and the scan rate was from 10 to 500 mV s^{-1} with the voltage range from 0 to 1.2 V referred to the saturated silver-chloride electrode. The voltammetric charges (q^*) corresponding to active surface areas was determined by integrating the area of the cyclic curve.

Impedance measurements were also performed with a PAR 273A potentiostat/galvanostat in above three-electrode configuration and were carried out using an EG&G-PARC model 5210 lock-in amplifier. The frequencies were scanned between 100 mHz and 100 KHz using the "single-sine" method. The experimental impedance data were fitted to an equivalent circuit using Wuhan University's EvolCRT software (Version 6.0).

The electrodes polarization and stability-test were measured in SPE cell at galvanostatic condition up to 1.1 A cm^{-2} at room temperature.

X-ray powder diffraction measurements were performed at room temperature using a D/max 2500 V PC X-ray diffractometer (Rigaku), with monochromatized Cu Kα radiation. Morphology and particle sizes were analyzed in a XL30 ESEM FEG (FEI Co.) field-emission scanning electron microscope (FE-SEM). The ruthenium contents in the liquid were determined by a POEMS (TJA Co.) inductively coupled plasma spectroscopy (ICP).

Nitrogen physical adsorption–desorption isotherms were performed with a micromeritics Asap model 2010 at 77 K. They were used to estimate specific surface area from BET.

3. Results and discussion

Fig. 1 shows XRD patterns of the RuO_2 powder after calcining at various temperatures (350–550 °C) for 15 h. As can be seen in the figure, all peaks match a rutile-structure RuO_2 as indexed. On the other hand, the RuO_2 peak intensity increased with further increase of the calcining temperature, indicating that the RuO_2 gradually crystallized and sintered at high temperature. The increase of calcining temperature result in the decrease of surface area of RuO_2 catalysts, which due to a result of RuO_2 particle sintering. This also confirmed by the decrease of BET surface area and increase of diameter of crystal size of samples with increase of calcining temperature (see Table 1). Moreover, the decrease of surface area with increase of crystallization tem-

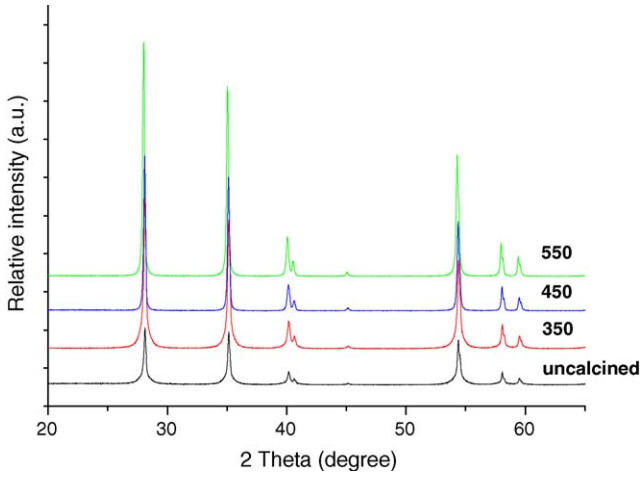

Fig. 1. XRD patterns of samples calcined at various temperatures.

Table 1
Impedance parameters for the double layer potential region and the oxygen evolution region obtained by fitting the experimental data to the equivalent circuit $R_s(R_fC_f)C_{dl}$ and $R_s(R_fC_f)(R_{ct}C_{dl})$

Samples	E ($V_{Ag/AgCl}$)	Unannealing	R350	R450	R550
BET surface area ($m^2\,g^{-1}$)	–	137	108	53	31
D[a] (nm)	–	34	37.5	43	48.2
R_f ($\Omega\,cm^{-2}$)	0.3	5.5	4.9	4.0	2.5
	1.4	0.45	0.329	0.272	0.173
R_s ($\Omega\,cm^{-2}$)	0.3	0.35	0.36	0.40	0.35
	1.4	0.34	0.35	0.40	0.34
R_{ct} ($\Omega\,cm^{-2}$)	1.4	10.0	17.5	22.0	40.0
C_f ($mF\,cm^{-2}$)	0.3	20.0	19.8	19.8	19.8
	1.4	11.2	12.4	20.0	15.0
C_{dl} ($mF\,cm^{-2}$)	0.3	19.2	18.6	17.6	17.4
	1.4	17.4	15.4	13.0	12.1

Electrodes prepared at different calcining temperature.
[a] The average crystallite sizes of RuO_2 is calculated according to Schrrer equation.

perature also reported by Ioroi et al. in the study of IrO_2/Pt electrocatalysts for unitized regenerative fuel cell [22].

In order to investigate the crystallization and sintering process of RuO_2 catalysts, a direct morphology observation was conducted. FE-SEM images of RuO_2 catalysts calcined at various temperatures are shown in Fig. 2. Any crystalline RuO_2 forms are not observed in uncalcined RuO_2 (Fig. 2A). SEM observation with high magnification for uncalcined RuO_2 (Fig. 2A, inset) showed that it appeared to consist of agglomerates of the 30–40 nm RuO_2 particles. SEM images of calcined samples (Fig. 2B–D) clearly showed that RuO_2 particles gradually agglomerating and crystallizing with increase of calcining temperature. The surface of RuO_2 catalyst after calcination at low temperature was much rougher than that after calcinations at high temperature. Thus, the RuO_2 catalyst after calcinations at low temperature has small particle size and larger surface areas, so it means that the more material near the center of the particles can be utilized.

Cyclic voltammograms for samples as porous electrode at 20 $mV\,s^{-1}$ are shown in Fig. 3. The irreversible peaks occurring around +0.5 V versus Ag/AgCl have been attributed to the valence state change of the metal oxide from 3+ to 4+ in the

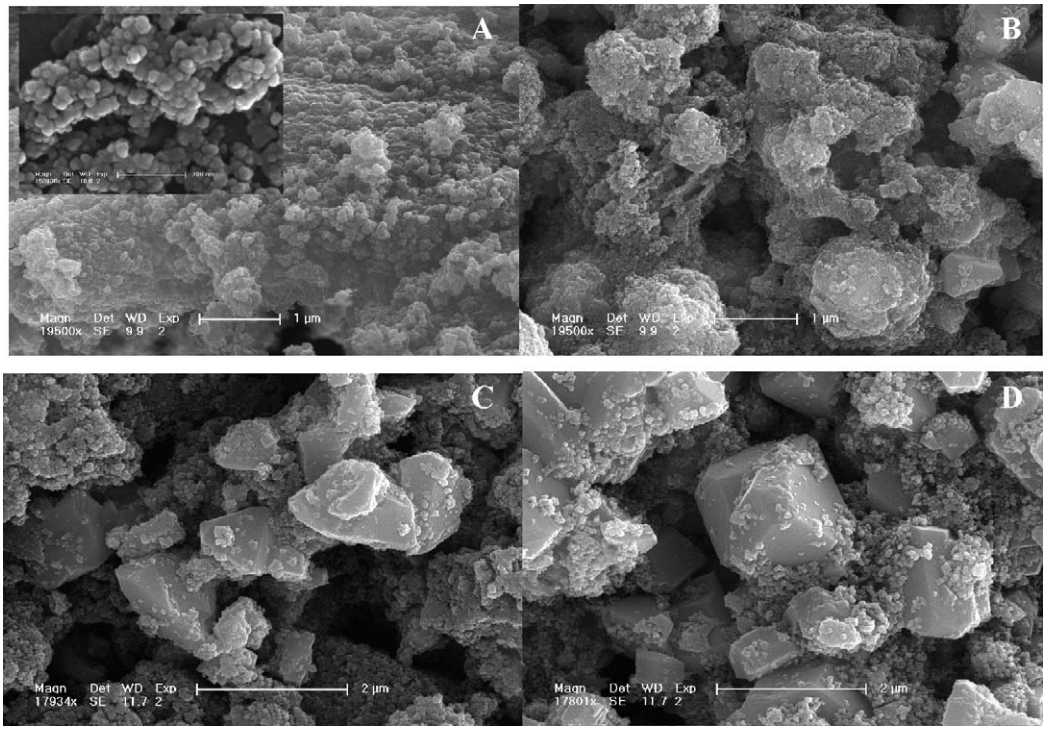

Fig. 2. FE-SEM images of samples prepared at various temperatures. (A) Uncalcined sample, (B) sample calcined at 350 °C, (C) sample calcined at 450 °C and (D) sample calcined at 550 °C.

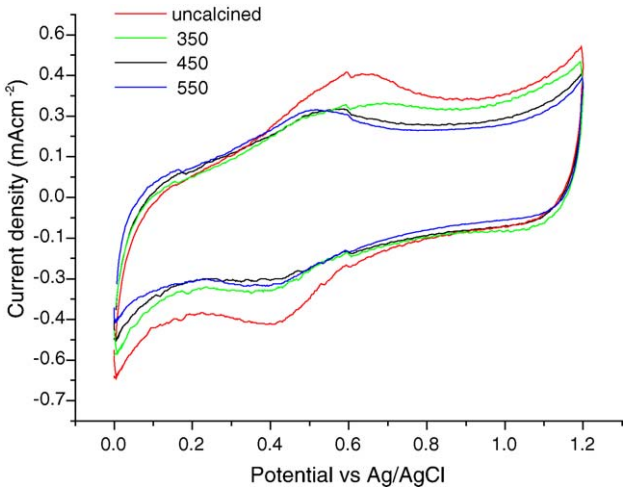

Fig. 3. Cyclic voltammograms of samples in 1 M H_2SO_4, at 20 mV s^{-1} and at room temperature.

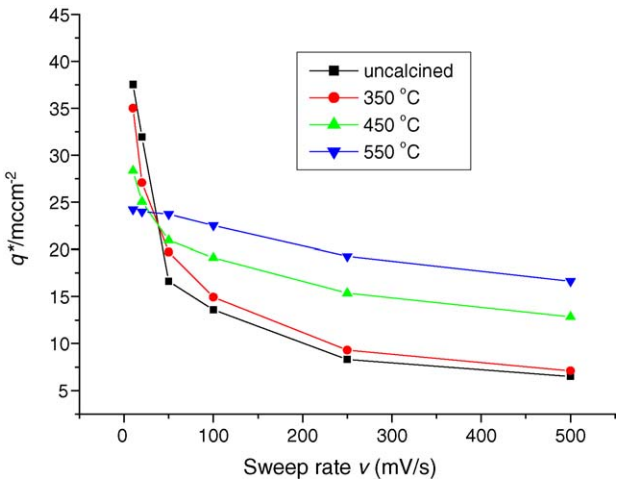

Fig. 4. Variation of q^* of electrodes calcined at different temperature with sweep rate.

RuO_2 [23]. Integration of the *j–E* curve provides the voltammetric charge q^*, which is proportional to the number of surface active sites. The change of q^* values of samples with sweep rate v are shown in Fig. 4. It is found that the q^* values of samples all decrease with increase of sweep rate v gradually. According to the investigation of some researchers [24,25], when sweep rate v smaller, the q^* value is related to the whole active surface. Conversely, when sweep rate v larger, the q^* value is related to outer active surface. Thus, the change of q^* values of samples at lower sweep rate also shows whole active surface of sample calcined at low temperature is much larger than that of sample calcined at high temperature. Moreover, when heat-treated temperature is higher, the change of q^* value of samples with sweep rate v is more flat. This phenomenon is attributed to the increase of outer active surface and the decrease of whole active surface of RuO_2 under higher heat-treated temperature. This is also in good agreement with the observation from SEM.

Electrochemical impedance spectroscopy (EIS) at constant potential 0.3 V (double layer region) and 1.4 V (oxygen evolution region) was used. The complex plane ($-Z_{image}$ versus Z_{real}) at a given potential 0.3 V for various samples is shown in Fig. 5A. The Nyquist plots of RuO_2 electrodes prepared at various temperatures for 0.3 V potential are characterized by two distinct regions. In the high frequency region, a short straight line with a lower angular coefficient is observed changing significantly with calcining temperature. A decrease in the frequencies caused a gradual change in the curve resulting in a second straight line with a higher angular coefficient observed in the low frequency domain. The high frequency intercept with the real axis almost is constant for all samples (as can be seen from Table 1). While the impedance behavior observed at low frequencies can be attributed to the oxide/electrolyte interface, the liner behavior observed in the high frequency domain may be related to the intrinsic properties of these materials. Similar

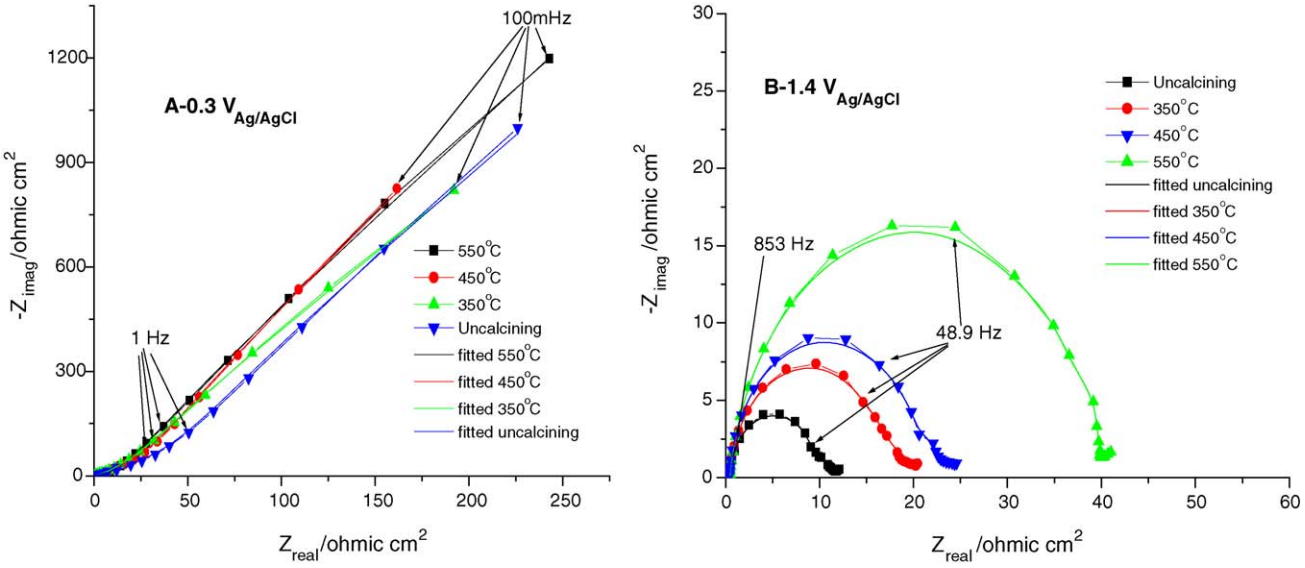

Fig. 5. Complex plane plots of RuO_2 catalysts as a function of calcining temperature, measured at (A) 0.3 $V_{Ag/AgCl}$ and (B) 1.4 $V_{Ag/AgCl}$, at room temperature.

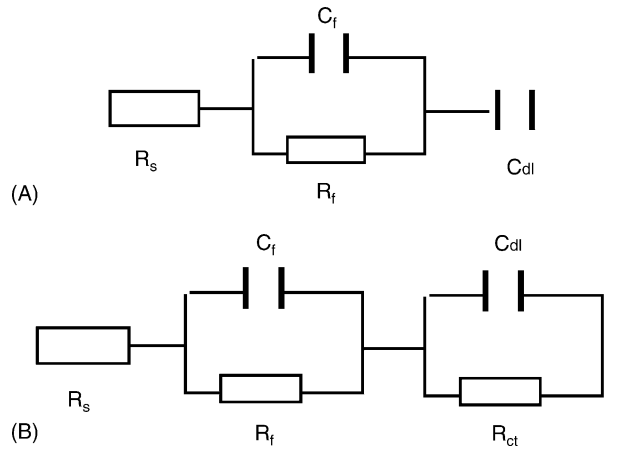

Fig. 6. Equivalent circuits (EC) used in the analysis of the experimental EIS data. (A) EC used in the double layer potential region (0.3 $V_{Ag/AgCl}$). (B) EC used in the oxygen evolution potential region (1.4 $V_{Ag/AgCl}$).

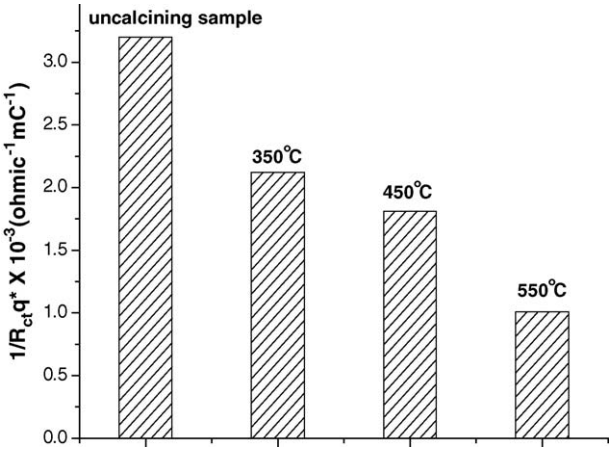

Fig. 7. Site activity, $1/R_{ct}q^*$, as a function of calcining temperature; $E = 1.4\ V_{Ag/AgCl}$.

impedance spectra have been observed for thermally prepared RuO_2-based electrodes [26–30]. The equivalent circuit model in Fig. 6A was used to analyze the EIS data. In this circuit the parallel (R_fC_f) combination takes into account the properties of the film, while the C_{dl} is associated with the oxide/electrolyte interface. R_s and R_f represent solution resistance and oxide film resistance, respectively. The parameters obtained by simulation are summarized in Table 1.

The OER impedance behavior was investigated in the potential region at 1.4 V. Fig. 5B shows representative Nyquist plots of the electrochemical impedance behavior, together with the data obtained by simulation using the equivalent circuit shown in Fig. 6B. Nyquist plots show that the diameter of the low frequency arc, which should be a measure of the polarization resistance and thereby of the catalytic activity of the electrode, is lowest for the uncalcining sample and increases continuously with increase of calcining temperature. These results are probably connected with the crystal growth of RuO_2 with increase of calcining temperature followed by a lower electrocatalytic activity. In Fig. 6B, this circuit the parallel (R_fC_f) combination takes into account the properties of the film, while the parallel ($R_{ct}C_{dl}$) combination is associated with the OER. R_s, R_f and R_{ct} represent solution resistance, oxide film resistance and charge transfer resistance for oxygen evolution, respectively. The parameters obtained by simulation are also summarized in Table 1.

It is found from Table 1 that R_Ω values between 0.3 and 0.4 $\Omega\,cm^2$, independent of calcining temperature and applied potentials are found. The film resistance (R_f) decreases with increase of calcining temperature, which can be attributed to the corresponding increased crystallinity of the oxide films, however, leads to an increase in the electrical conductivity. Charge transfer resistance (R_{ct}) as a function of calcining temperature increases with increase of calcining temperature, suggest the uncalcining RuO_2 is the most efficient for the OER. The further increase of R_{ct}, observed at the higher calcining temperature, is associated with a more extensive sintering occurring at the higher calcining temperature, as a result of which a lower number of active sites is exposed to the solution. This observation is in agreement with the behavior of C_{dl} (see Table 1) as a function of the calcining temperature, as evidenced by SEM and CV.

In fact, R_{ct} is proportional to the product of the number of active sites and the site activity [31]. Thus, to obtain information with respect to the real electrocatalytic activity of the several materials, R_{ct} values must be normalized for morphological effects. According to some authors [32,33], this can be done dividing $1/R_{ct}$ (overall electrode activity) by the number of active sites (q^*) or $1/R_{ct}q^*$ [32,33]. The $1/R_{ct}q^*$ data show highest site activity is found for uncalcining sample, while a poorer performance for the OER in acidic medium is observed for the other samples prepared at higher calcining temperature (see Fig. 7). This behavior of $1/R_{ct}q^*$ as a function of calcining temperature reveal that the calcining conditions have a considerable effect on the properties of the catalytic layers.

Steady-state polarization curves for uncalcined material and for samples calcined at temperatures ranging from 350 to 550 °C are shown in Fig. 8. The potentials are not corrected for IR

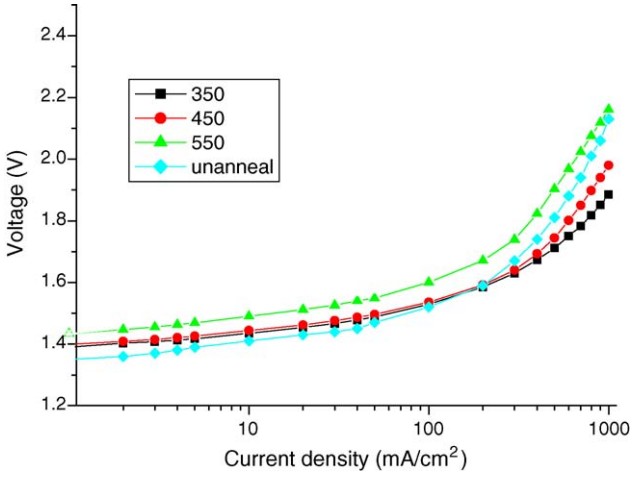

Fig. 8. Steady-state cell polarization curves as a function of different calcined temperature of RuO_2 catalyst during oxygen evolution.

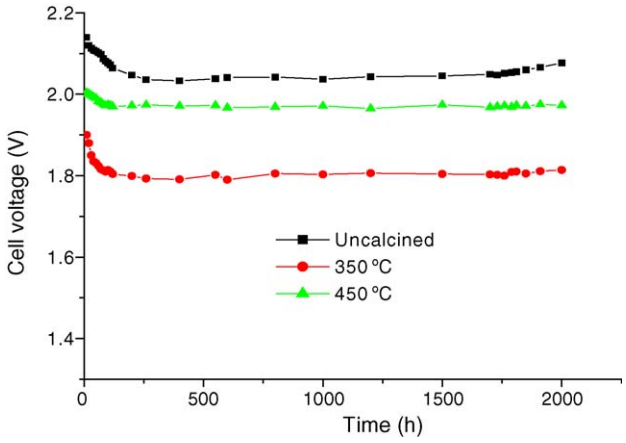

Fig. 9. Change of cell voltage with electrolysis time for RuO_2 anode at 1100 mA cm^{-2} in SPE cell.

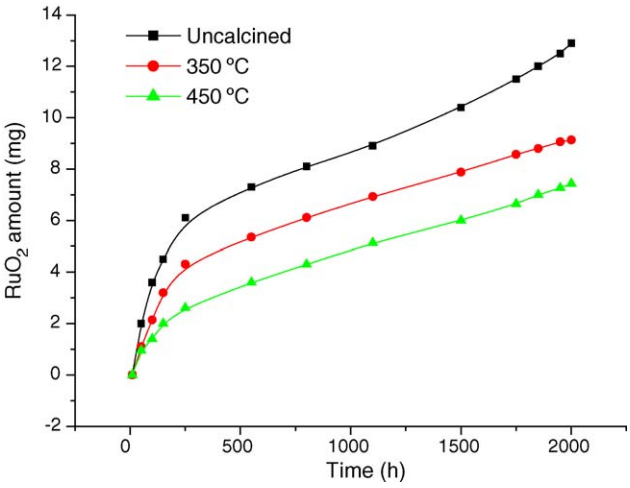

Fig. 10. Change of RuO_2 amount in water during electrolysis at 1100 mA cm^{-2} in SPE cell.

drops. At low current densities the uncalcined material exhibits the best catalytic properties with the lowest total overpotential for OER. The potential then increases with increase of calcining temperature. At high current densities, above 200 mA cm^{-2}, the potential of OER for uncalcined sample exceeds that of samples prepared at 350 and 450 °C and with a very steep rise of the slope of the curve. These results show that the catalytic properties of the material are governing the potential for OER at low current densities, whereas the resistance of the catalyst layer (R_f) determines the potential for OER at high current densities. This means that an optimum heat-treated temperature is found at 350 °C where the total anodic potential in the high current densities range of 0.2–1.1 A cm^{-2} is lowest.

The results of stability-test for electrodes calcined at different temperature are presented in Fig. 9. The electrolysis time of 2000 h has been ran at room temperature with 1100 mA cm^{-2} of applied current density. The cell voltage decreases during the initial stage of the electrolysis, which can be attributed to the wetting of less accessible inner surface of the oxide electrode due to its porous nature [34,35]. The cell voltage is then stable for a long period, and finally only cell voltage of uncalcined sample has the slow rises-trend was observed. In general, the deactivation of this type of electrodes is usually associated with the coating dissolution during electrolysis [36]. The losing amounts of RuO_2 for electrodes calcined at different temperature in electrolysis are presented in Fig. 10. The losing amounts of RuO_2 for these electrodes rises abruptly during the initial stage of the electrolysis, which can be attributed to preferred-dissolution of "irregular" coating in porous structure RuO_2. The dissolution of RuO_2 electrodes calcined at different temperature is then mild for a very long time, and only the dissolution rate of uncalcined RuO_2 electrode was more rapid. Similar results also obtained by Krysa et al. [37,38] in the study of dissolution of IrO_2 electrodes during the accelerated life-tests. Because the dissolution of RuO_2 is slow and the question of oxidation of Ti substrate is not existing, the stability of electrodes is better and the cell voltage is not rising abruptly. Furthermore, this result also reveals that RuO_2 electrode calcined at higher temperature has higher corrosion resistance.

4. Conclusion

Above study revealed that the catalytic performance of the catalyst for OER is related with the heat treatment of material. RuO_2 particle size increases and the material becomes more crystalline with increase of calcining temperature, leading to lower electrochemical active surface and higher electronic conductivity. There seem to exist both positive and negative related to the effect of calcining temperature on the OER performance of the catalysts. Thus, optimum calcining conditions were found at 350 °C in this work.

Acknowledgements

This work was supported by 973 Program (G2000026408), 863 Program (2001AA323060, 2003AA517060) of Science and Technology Ministry of China, The National Natural Science Foundation of China (General Program 20373068, Key Program 20433060), Natural Science Foundation of Jilin Province (20000510).

References

[1] D.M. Novak, B.V. Tilak, B.E. Conway, in: J.O'M. Bockris, B.E. Conway, R.E. White (Eds.), Modern Aspects of Electrochemistry, vol. 14, Plenum Press, New York, 1982, pp. 195–222.
[2] S. Trasatti, G. Buzzanca, J. Electroanal. Chem. 29 (1971) 1.
[3] S. Trasatti, Electrochim. Acta 45 (2000) 2377.
[4] F. Cardarelli, P. Taxil, A. Savall, Ch. Comninellis, G. Manoli, O. Leclerc, J. Appl. Electrochem. 28 (1998) 245.
[5] M. Morimitsu, H. Tamura, M. Matsunaga, R. Otogawa, J. Appl. Electrochem. 30 (2000) 511.
[6] S. Kulandaisamy, J.P. Rethinaraj, S.C. Chockalingam, S. Visvanathan, K.V. Venkateswaran, P. Ramachandran, V. Nandakumar, J. Appl. Electrochem. 27 (1997) 579.
[7] R. Mraz, J. Krysa, J. Appl. Electrochem. 24 (1994) 1262.
[8] C. Bock, H. Spinney, B. MacDougall, J. Appl. Electrochem. 30 (2000) 523.
[9] J.M. Sedlak, R.J. Lawrance, J.F. Enos, Int. J. Hydrogen Energy 6 (1981) 159.

[10] P. Millet, M. Pineri, R. Durand, J. Appl. Electrochem. 19 (2) (1989) 162–166.
[11] Y. Nishimura, K. Yasuda, Z. Siroma, K. Asaka, Denki kagaku oyobi kogyo butsuri kagaku 65 (12) (1997) 1122–1123.
[12] W. Kreuter, H. Hofmann, Hydrogen Energy Prog. XI 1 (1996) 537.
[13] C. Mitsugi, A. Harumi, F. Kenzo, Int. J. Hydrogen Energy 23 (1998) 159.
[14] H. Mori, C. Inazumi, M. Kato, S. Maezawa, K. Oguro, H. Takenaka, E. Torikai, Hydrogen Energy Prog. XI 1 (1996) 579.
[15] M. Kondoh, N. Yokoyama, C. Inazumi, S. Maezawa, N. Fujiwara, Y. Nishimura, K. Oguro, H. Takenaka, J. New Mater. Electrochem. Syst. 3 (2000) 61.
[16] S. Stucki, G.G. Scherer, S. Schlagowski, E. Fischer, J. Appl. Electrochem. 28 (1998) 1041.
[17] B. Børrensen, G. Hagen, R. Tunold, Electrochim. Acta 47 (2002) 1819.
[18] R. Adams, R.L. Shriner, J. Am. Chem. Soc. 45 (1923) 2171.
[19] L. Giorgi, A. Pozio, E. Antolini, E. Passalacqua, Electrochim. Acta 43 (1988) 3675.
[20] E. Antolini, L. Giorgi, A. Pozio, E. Passalacqua, J. Mater. Sci. 33 (1998) 1837.
[21] A. Marshall, B. Børresen, G. Hagen, M. Tsypkin, R. Tunold, Norwegian Hydrogen Seminar, Kvitfjell, 2004.
[22] T. Ioroi, N. Kitazawa, K. Yasuda, Y. Yamamoto, H. Takenaka, J. Electrochem. Soc. 147 (6) (2000) 2018–2022.
[23] K. Dobelhofer, M. Metikos, Z. Ogumi, H. Gerischer, Ber. Bunsenges. Phys. Chem. 82 (1978) 1046.
[24] S. Ardizzone, G. Fregonara, S. Trasatti, Electrochim. Acta 35 (1990) 263.
[25] C. Angelinetta, S. Trasatti, L.D. Atanasoska, R.T. Atanasoska, J. Electroanal. Chem. 214 (1986) 535.
[26] K.C. Liu, M.A. Anderson, J. Electrochem. Soc. 143 (1996) 124.
[27] L.A. Da Silva, V.A. Alves, M.A.P. Da Silva, S. Trasatti, J.F.C. Boodts, Electrochim. Acta 42 (1997) 271.
[28] D. Tswen Shieh, B.J. Hwang, Electrochim. Acta 38 (1993) 2239.
[29] I.R. Burrows, D.A. Denton, J.A. Harrison, Electrochim. Acta 23 (1978) 493.
[30] T.A.F. Lassali, J.F.C. Boodts, L.O.S. Bulhões, Electrochim. Acta 44 (1999) 4203.
[31] Y.L. Lo, B.J. Hwang, J. Electrochem. Soc. 143 (1996) 2158.
[32] B.J. Hwang, D.T. Shieh, A.S.T. Chang, J. ChlChE 25 (1994) 127.
[33] D.T. Shieh, B.J. Hwang, J. ChlChE 25 (1994) 87.
[34] M. Morimitsu, H. Tamura, M. Matsunaga, R. Otogawa, J. Appl. Electrochem. 30 (2000) 511.
[35] S. Trasattti, Electrochim. Acta 36 (1991) 225.
[36] C. Iwakura, K. Hirao, H. Tamura, Electrochim. Acta 22 (1977) 329.
[37] J. Krysa, L. Kule, R. Mraz, I. Rousar, J. Appl. Electrochem. 26 (1996) 999.
[38] R. Mraz, J. Krysa, J. Appl. Electrochem. 24 (1994) 1262.